



# Shear-coupled grain boundary migration in bicrystal Ni with metallic dopant segregation

Jie Li<sup>1</sup>, Xinhua Yang<sup>1,2,a)</sup>, Peng Wang<sup>3</sup>

<sup>1</sup>School of Aerospace Engineering, Huazhong University of Science and Technology, Wuhan 430074, China

<sup>2</sup>Hubei Key Laboratory of Engineering Structural Analysis and Safety Assessment, 1037 Luoyu Road, Wuhan 430074, China

<sup>3</sup>College of Engineering, Huazhong Agricultural University, Wuhan 430070, China

<sup>a)</sup>Address all correspondence to this author. e-mail: yangxinh@hust.edu.cn

Received: 1 September 2020; accepted: 24 November 2020; published online: 2 January 2021

The shear-coupled grain boundary (GB) migration in bicrystal Ni with metallic dopant segregation was investigated by the molecular dynamics simulations. Different from the approximately linear relation of the GB migration of pure bicrystal Ni with the nominal shear strain, the curve of doped bicrystal Ni can be divided into three stages. The threshold strain, saturated strain, and saturated GB migration displacement can be used to characterize them. They are considerably affected by the Cr concentration in GB, temperature, and dopant type. The higher the dopant concentration is or the lower the temperature is, the greater the resistance to GB migration is. Cu dopant induces the greatest resistance, Cr and Fe dopants have great effect on the GB migration, but Co has almost no influence. All these hindering effects can be explained from the variation of the number of pinning points induced by the dopant atoms in GB.

## Introduction

Grain boundaries (GBs) have a great influence on the mechanical properties of materials. The increase of GBs in volume content can improve strength and hardness of nanocrystalline materials [1–3], so grain refinement becomes a powerful tool to design materials with superior mechanical properties and performance. On the other hand, nanocrystalline materials generally have poor thermal stability, because high GB energies would provide the driving force for grain growth [4–6]. As a result, the advantages from high GB volume content possibly disappear as the grains grow up.

GB structures can be stabilized by alloying nanocrystalline materials [7, 8]. The high temperature stability of nanostructured W-Ti alloy was demonstrated to be substantially enhanced [9]. It is worth noting that alloying atoms are easily segregated into GBs and GB segregation can lead to structural transformation inside GBs. Much attention was paid to the experimental investigations of GB segregation in Ni [10–14]. It was found that GB segregation can lead to intermediate temperature embrittlement [13], introduce a new mechanism of high temperature stability [14], and control grain size by doping content [10]. Molecular dynamics (MD) simulations have been also used to study significant effects of GB segregation on material properties. For example, GB segregation can induce

an obvious increase in the strength of nanocrystalline [15, 16] and nanocomposites [17] and improvement in the creep resistance of metallic materials [18, 19]. As a kind of interfacial phase transition, the GB complexions were studied by doping Ag in Cu [20], Ni in Mo [21], and Zr and Ag in Cu [22]. The GB complexions were found to play a complicated role in the creep behavior of materials [23]. In addition, different metallic dopants were also found to have different effects on the GB embrittlement of Mo [24].

Shear-coupled GB migration, as a mechanism of grain growth, was studied theoretically [25–27] and numerically [28–34]. Wan et al. [29] investigated the shear response of the  $\Sigma 9 < 110 > \{221\}$  symmetric tilt GB in face-centered-cubic (FCC) metals Cu, Al, and Ni by atomistic simulations and observed the elementary structure transformations during GB migration. Furthermore, the GB migration in nanocrystalline materials can be much more complicated due to the pinning effect of triple junctions [33, 34].

Segregating dopants in GB could retard GB mobility [35–37] and inhibit the shear-coupled GB migration [38, 39]. It is not clear how GBs are hindered and how GB structures evolve during migration affected by dopant segregation. Atomic-scale observations of GB migration behavior via MD simulations can help to answer above questions. In this paper, the GB migration

behaviors of bicrystal Ni with different types and concentrations of dopant atoms are simulated at different temperatures, monotonically increasing shear strain. The underlying physical mechanism, by which the dopant segregation inhibits GB migration, as well as the effects of dopant atom type, concentration, and temperature, is investigated.

## Results and discussions

### Characteristic parameters

In order to investigate the migration behavior quantitatively, the GB migration displacement versus nominal shear strain curve for 10 at.% Cr-doped bicrystal Ni is plotted in Fig. 1 by a solid line. For comparison, the migration displacement curve of pure bicrystal Ni is also plotted in Fig. 1 by a marked line.

It can be seen that the pure Ni curve is always approximately linear but the 10 at.% Cr-doped Ni curve obviously has three stages. In stage I with shear strain less than 5.5%, the 10 at.% Cr-doped Ni curve overlaps almost exactly with the pure Ni curve. It indicates that Cr dopant has very little impact on GB migration in this case. In stage II with shear strain from 5.5 to 17%, the curve slope is reduced. This indicates that GB migration is hampered. The curve is separated from the pure Ni curve although it can also be approximately described with a linear relationship, as shown in Fig. 1 by a dotted line. The shear strain at the start point of stage II can be called the threshold strain  $\gamma_{th}$ . Only when the shear strain is larger than it, does Cr dopant have effect on the GB migration. Finally, when the shear strain is larger than 17%, the 10 at.% Cr-doped Ni curve enters stage III and its GB migration displacement reaches saturation. Thus, the shear strain at this point and its corresponding migration displacement can be called saturated shear strain and saturated

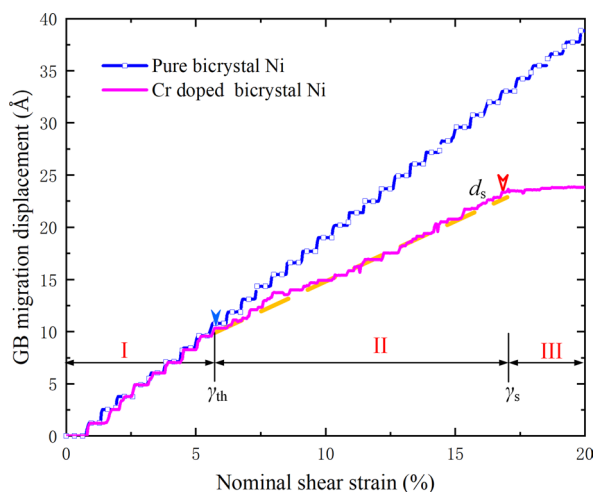


**Figure 1:** GB migration displacement versus nominal shear strain curves for pure bicrystal Ni and 10 at.% Cr-doped bicrystal Ni.

GB migration displacement, respectively. They are denoted as  $\gamma_s$  and  $d_s$ , respectively. The two segment points are indicated by the solid and dotted arrows in Fig. 1, respectively.

To reveal the physical mechanisms hiding behind the aforementioned phenomena, some questions need to be clarified. (1) Why can dopant segregation pin the GB? In fact, it was found early that dopant segregation could reduce the GB energy and enhance the GB cohesion to strengthen the migration resistance of the GB near dopants [7, 40–42]. As a result, only when doped atoms are gathered locally to a certain degree, the GB near them would be pinned. (2) Why does there exist a threshold effect in the hindering effect of Cr dopants? Fig. 2a and b show the GB atomistic configuration at 5.5% shear strain for the pure and doped bicrystals, respectively. It can be seen that the GB is kept in order in the pure bicrystal during migration but two pinning points A and B form where the dopant atoms gather in the doped bicrystal. The GB segments in the both sides of A and B become disordered or change their elementary structures, as marked by the dotted ellipses in Fig. 2b. Since GB migration is achieved through the transformation of elementary structural units [25, 29, 31], the length of disordered GB can be used to indicate the magnitude of the resistance to migration. Only when this length accumulates to a certain proportion, the hindrance to GB migration becomes significant, which the threshold strain corresponds roughly to this proportion. From Fig. 1, it also proves that the dopants do not hinder the GB to migrate when the disordered GB is shorter than that corresponding to the threshold strain. (3) Why do the dopants hinder the GB to migrate in stage II? Fig. 2c shows the GB atomistic configurations at 10% shear strain for the doped bicrystal. The GB disordered segments become longer with increasing shear strain when the shear strain is larger than the threshold strain. As a result, the GB migration behavior becomes more difficult to occur. (4) Why does the GB migration reach saturation in stage III? Fig. 2d shows the GB atomistic configurations at the saturated strain for the doped bicrystal. The GB segment between A

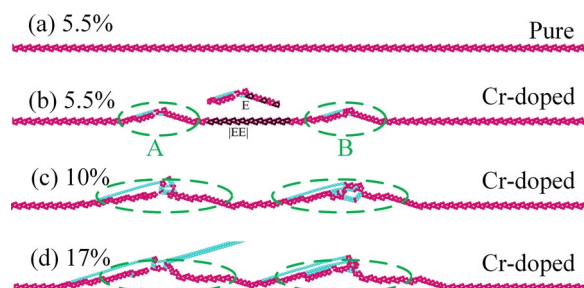


**Figure 2:** GB atomistic configurations at nominal shear strain of (a) 5.5% for the pure bicrystal Ni and (b) 5.5%, (c) 10%, and (d) 17% for the Cr-doped bicrystal Ni.

and B completely becomes disordered, so that it stops migrating. In other words, the GB migration starts to saturate at this moment.

The dopant atoms hinder the GB to migrate when they get together to form the pinning points in the GB. Figure 3 shows the GB atomic configuration evolution around pinning point A with the shear strain increasing from 2.4 to 6.2%. In Fig. 3a, for shear strain of 2.4%, a GB disconnection occurs firstly at point A due to some dopant atoms gathering here. GB disconnections are topological defects with step and dislocation characteristics constrained to crystal interface [43]. Their nucleation and motion are important mechanisms of shear-coupled GB migration [44, 45]. However, the disconnection at point A cannot move and begins to stop the transformation of nearby structural units due to pinning. With increasing shear strain, more GB disconnections pile up near point A and more structural units cannot be transformed. As a result, the length of the disordered GB segment increases from 8 Å in Fig. 3b to 30 Å in Fig. 3c, 49 Å in Fig. 3d, 62 Å in Fig. 3e, and 72 Å in Fig. 3f, when the shear strain increases from 2.6 to 3.3%, 4.5%, 5.2%, and 6.2%. In the meantime, the number of |EE| structural units outlined is gradually decreased. The impact of the pinning point on GB migration is generally similar to that of the triple junctions making the GB from order to disorder [33].

The threshold strain  $\gamma_{th}$ , the saturated strain  $\gamma_s$  and the saturated migration displacement  $d_s$  can be treated as the characteristic parameters for the GB migration behavior in doped bicrystal Ni. And they could also be affected by dopant concentration, temperature and dopant type [38].

### Effect of dopant concentration

To investigate the effect of dopant concentration on the GB migration behavior, the Cr concentration in the GB was changed from 0 to 20 at.% with an increment of 2 at.%. In the range of 20% shear strain, all the GB migration curves for the Cr concentration cases of 2 at.%, 4 at.% and 6 at.% overlap with that of pure Ni bicrystal, and the 14% at.% and 18 at.% Cr concentration cases have GB migration curves similar to the 16 at.% Cr concentration case. For clarity and brevity, Fig. 4 only plots the GB migration displacement versus nominal shear strain curves for the seven cases with Cr concentration of 0, 4 at.%, 8 at.%, 10 at.%, 12 at.%, 16 at.% and 20 at.%. Apparently, the 4 at.% Cr concentration curve nearly coincides with the pure Ni curve, which means that the GB migration is hardly affected by Cr concentration when it is lower. When the Cr concentration reaches 8 at.%; however, the curve starts to separate from the pure Ni curve at 14% shear strain and enters into stage II of GB migration. Therefore, 14% can be regarded

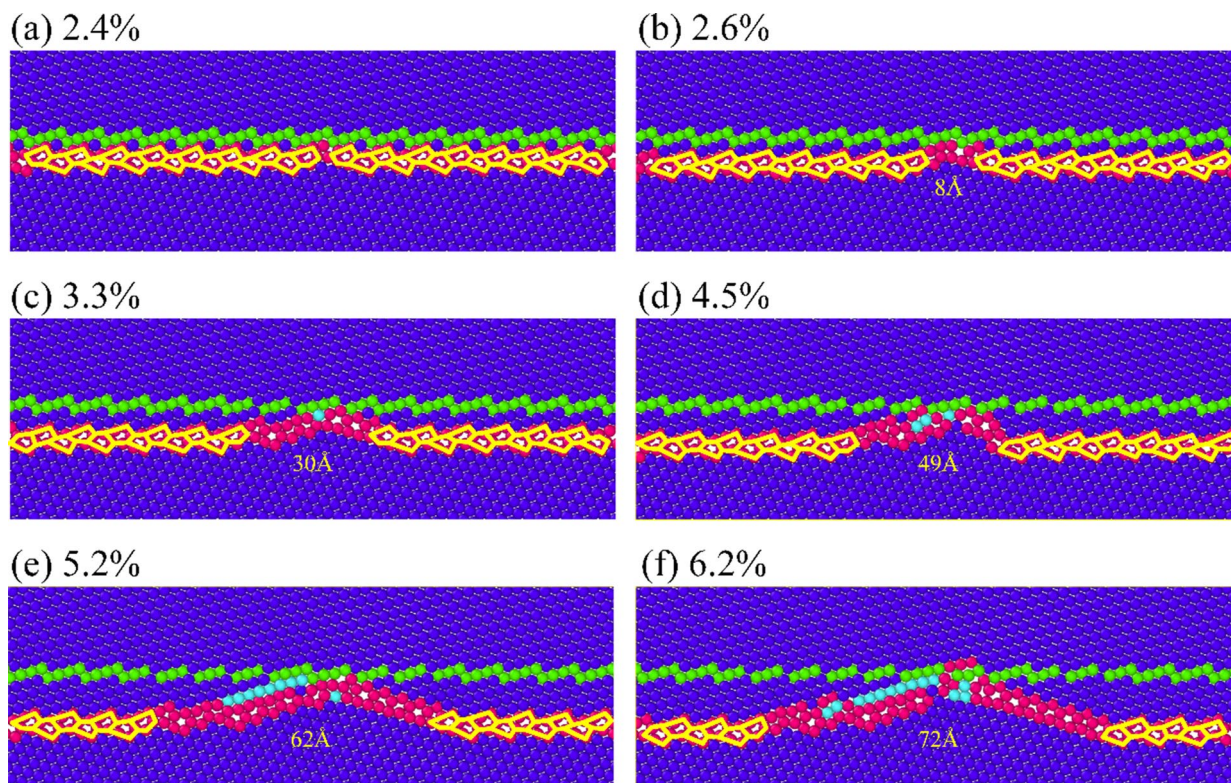


**Figure 3:** GB atomic configurations near pinning point A in the doped bicrystal for shear strains of (a) 2.4%, (b) 2.6%, (c) 3.3%, (d) 4.5%, (e) 5.2%, and (f) 6.2%.



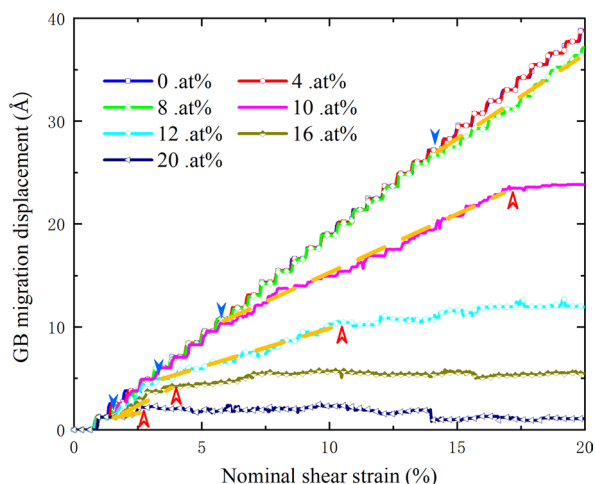


**Figure 4:** GB migration displacement versus nominal shear strain curves for different Cr concentrations in GB.

as the threshold strain for the 8 at.% Cr concentration bicrystal. When the Cr concentration increases to 10 at.%, the threshold strain reduces to about 5.5% and the GB migration displacement saturates at about 17% shear strain. When the Cr concentration is 12 at.%, the threshold strain and saturated shear strain are about 3% and 10.5%, respectively. When the Cr concentration further increases to 16 at.%, the threshold strain and saturated shear strain reduces to about 1.5% and 3.5%, respectively. Finally, when the Cr concentration reaches 20 at.%, the two segment points are about 1.5% and 2.5%, respectively. They have been very close to each other. It should be pointed out that it is difficult to separate the migration curves into three regions exactly, so the above parameters of the segment points are approximate.

It is noted from Fig. 4 that the GB migration is not hampered for the 4 at.% Cr concentration case and there is no saturation stage for the 8 at.% Cr concentration case. In order to check if they are due to too small shear strain, both the two cases were calculated and these phenomena can be kept until the shear strain reached 30%.

To quantify the effect of Cr concentration, Fig. 5 plots the variations of the threshold shear strain, saturated shear strain and saturated GB migration displacement with the Cr concentration. It can be seen that all of them decrease monotonically as the Cr concentration increases, and their rates are rather high in the low Cr concentration zone, and then slowed down in the rest. In addition, the spacing between the saturated shear strain and the threshold shear strain rapidly decreases with increasing Cr concentration. This means that the higher the Cr concentration in GB is, the greater the GB migration resistance is. The relations of the threshold shear strain, saturated shear strain and

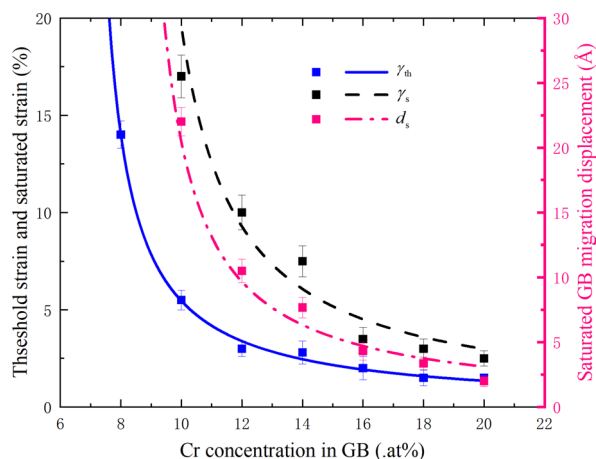


**Figure 5:** Variations of the threshold shear strain, saturated shear strain, and saturated GB migration displacement with the Cr concentration.

saturated GB migration displacement with the Cr concentration are fitted as follows,

$$\gamma_{th} = \frac{17.9}{c - 6.721} \quad (1)$$

$$\gamma_s = \frac{35.24}{c - 8.2} \quad (2)$$

$$d_s = \frac{36.77}{c - 8.2} \quad (3)$$

where  $c$  represents the Cr concentration in GB. They indicate that only when the Cr concentration is higher than about 6.721 at.% can the GB migration be hindered, and only when the Cr concentration is higher than about 8.2 at.% can the GB migration reach saturation. When the doped concentration is smaller than 8.2 at.%, the degree of gathering of doped atoms in GB is too low to form the pinning able to reach GB migration saturation.

In order to analyze the internal mechanism of the influence of Cr concentration on GB migration, the GB atomic configurations at 14% shear strain are shown in Fig. 6a–e for different Cr concentrations in GB, respectively. The horizontal lines in the figure represent the initial position of the GB. While the GB in Fig. 6a remains flat and orderly, one and three pinning points are formed as marked by the dotted ellipses in Fig. 6b and c, respectively. It can be seen that more pinning points appear when the Cr concentration increases to 16 at.% and 20 at.%, as shown in Fig. 6d and e. In general, the more the pinning points are, the longer the total length of disordered GB segments is, the greater the resistance to GB migration is. As a result, a GB with higher Cr concentration has a less threshold strain, a less saturated strain and a less saturated migration displacement.

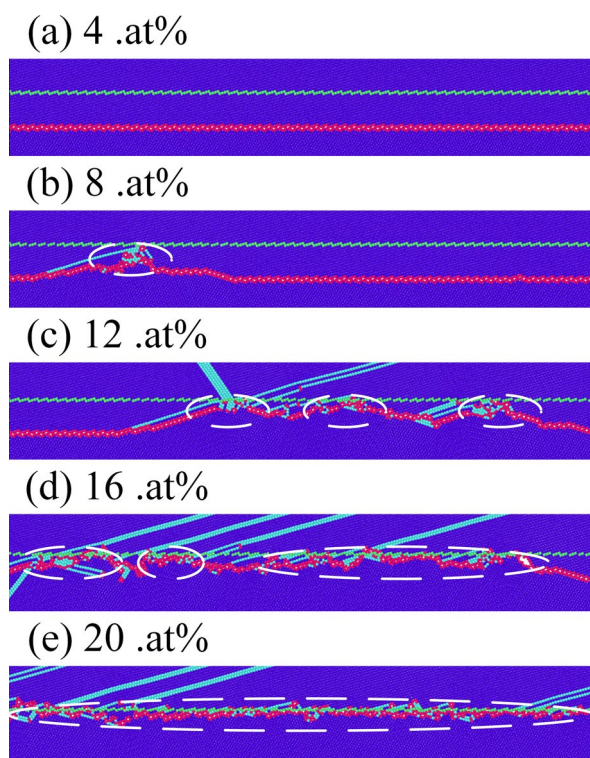


Figure 6: Configurations at the shear strain of 14% for Cr concentrations of (a) 4 at.%, (b) 8 at.%, (c) 12 at.%, (d) 16 at.%, and (e) 20 at.% in GB.

### The effect of temperature

To evaluate the effect of temperature on GB migration, the Cr concentration in GB was kept at 10 at.% but the temperature was changed from 1 K, to 10 K, 20 K, 50 K and 100 K. The shear-induced GB migration simulations were performed. The migration displacement versus nominal shear strain curves are plotted in Fig. 7 for different temperatures. It can be seen that the 50 K and 100 K curves are approximately linear within the scope of 20% shear strain, but when the temperature is less than 20 K, the bifurcation begins. The threshold strain at the segment points increases gradually with the temperature increasing from 1 to 20 K. When the temperatures are 1 K and 10 K, the GB migration saturates at about 15.5% and 17% shear strain, respectively. They indicate that the higher the temperature is, the less the hindering effect of dopant segregation is.

The effect of temperature on GB migration is realized by the influence on the number of pinning points. As the temperature increases, the number of pinning points in the models decreases due to thermal activation. The atomistic configurations at shear strain of 6% and temperatures of 1 K, 10 K, 20 K and 50 K are shown in Fig. S1 in the Supplementary Material. As a result, the higher the temperature is, the less resistance to GB migration is. It is worth noting that this trend should be applicable, though the temperature range selected here is small.

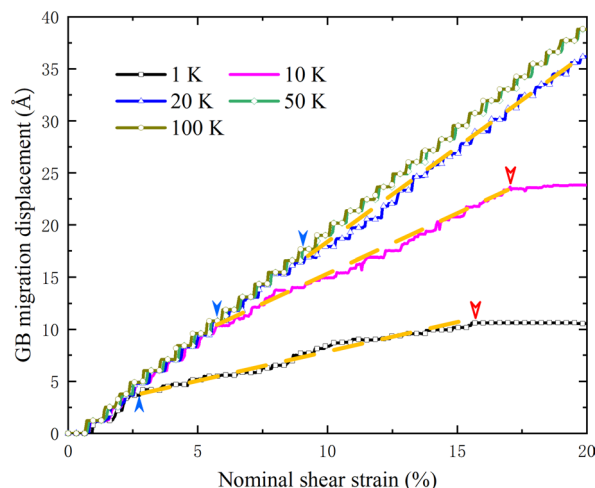


Figure 7: GB migration displacement versus nominal shear strain curves of the 10 at.% Cr concentration model for different temperatures.

### The effect of metallic dopant type

In order to evaluate the effect of metallic dopant type on GB migration, some simulations were also performed on the Fe, Cu, and Co dopant models. The dopant concentration was kept at 10 at.% and 20 at.%, respectively, and the temperature was at 10 K. Figure 8a and b show their GB migration versus nominal shear strain curves for 10 at.% and 20 at.% dopant concentration, respectively. For comparison, the curves of the 10 at.% and 20 at.% Cr dopant models and the pure Ni model are also given in this figure. It can be seen that the 10 at.% and 20 at.% Co dopant models have curves nearly coinciding with the pure Ni curve, while the GB migration is inhibited to different degrees for all the other dopant models. For 10 at.% dopant concentration, the threshold shear strains corresponding to Cu, Cr and Fe dopant models are about 2%, 5.5% and 7%, respectively. Thus,

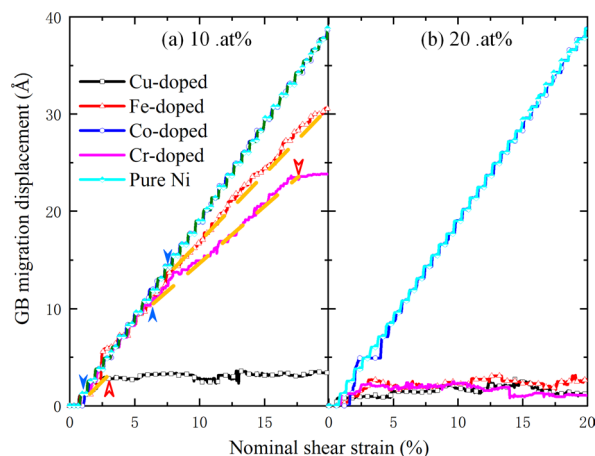


Figure 8: GB migration displacement versus nominal shear strain curves for (a) 10 at.% and (b) 20 at.% dopant concentrations.

the Cu dopant model has the greatest resistance, and the Cr dopant model has larger resistance than the Fe dopant model. However, when the dopant concentration reaches 20 at.%, all the Cu, Cr, and Fe dopant models are saturated in the GB migration almost from the beginning.

The GB segregation of doped atoms in Ni has been studied using first principles [46–50]. It was found that the GB segregation of doped atoms can strengthen the GB [46]. In general, the segregation tendency is closely related to the size mismatch between the dopant and host atoms [47, 48]. The interactions between the dopant and host atoms would lead to different positive heat of mixing. Doped atoms of different types have different atomic sizes. The heat of mixing between Cu and Ni atoms is much larger than that between the other three types and Ni atoms [51]. The influence of dopant atoms on GB motion can be attributed to the difference of mixing heat [38, 52]. Therefore, the hindering effect of doped Cu on GB motion is much more significant.

To reveal how the type of dopant atoms influences the GB migration behavior, the atomistic configurations of the 10 at.% Fe, Cr, Cu, and Co dopant models at shear strain of 6% and temperature of 10 K are shown in Fig. S2 in the Supplementary Material, respectively. In general, different doped atom types will affect the number of pinning points, and then affect its hindering effect on GB motion.

## Conclusions

The shear-coupled GB migration in bicrystal Ni with metallic dopant segregation was simulated using the molecular dynamics method. The following conclusions are obtained.

- (1) Different from pure bicrystal Ni, the GB migration in Cr-doped bicrystal Ni can be separated into three stages. The GB migration is hindered in stage II and eventually reaches saturation in stage III. The threshold strain, saturated strain and saturated GB migration

displacement can be used to characterize the GB migration behaviors of Cr-doped bicrystal Ni.

- (2) All the Cr concentration in GB, temperature and dopant type have considerable effects on the GB migration in bicrystal Ni with metallic dopant segregation. A higher dopant concentration or lower temperature leads to a greater resistance to GB migration. Among Cr, Fe, Cu, and Co dopants, Cu dopant induces the greatest resistance, but Co does the least.
- (3) All the effects of Cr concentration in GB, temperature and dopant type on the GB migration in bicrystal Ni with metallic dopant segregation can be attributed to the variation of the number of pinning points induced by the dopant atoms in GB.

## Model and simulation method

A quasi-three-dimensional atomic model of bicrystal Ni was created with a horizontal  $\Sigma 9 < 110 > \{221\}$  symmetric tilt GB in its middle. A Cartesian coordinate system was given with X, Y, and Z axes in the  $[114]$ ,  $[22\bar{1}]$  and  $[\bar{1}10]$  directions. The model has outline dimensions of 493 Å, 140 Å and 20 Å along the X, Y, and Z directions, respectively.

To quantitatively study the effect of GB segregation on migration behavior and avoid the effects of intragranular doped atoms, atoms at GB were randomly replaced by the doped atoms with concentrations from 0 to 20 at.%. Then the models were relaxed at 300 K for 100 ps to achieve both mechanical and chemical equilibrium. Subsequently, the models were slowly dropped to the desired temperature and relaxed for another 100 ps. Figure 9 shows the relaxed configuration of the Ni bicrystal model doped with 10 at.% Cr atoms in the GB at 10 K. It can be seen from the enlarged subgraph of Fig. 9 that the elementary structure of GB is not broken after the Cr atoms are doped. To eliminate local effect of data statistics, five areas with 80 Å spacing in the GB, shown with the boxes in Fig. 9, are

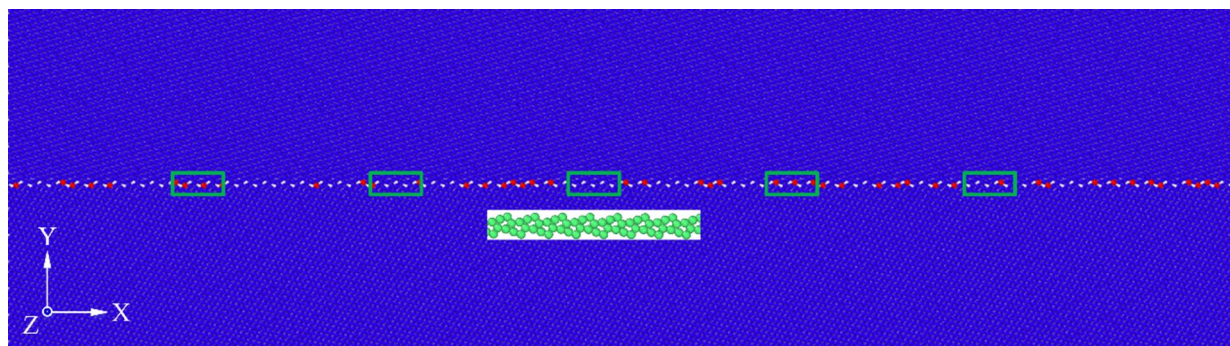


**Figure 9:** Bicrystal Ni model doped with 10 at.% Cr atoms in GB.



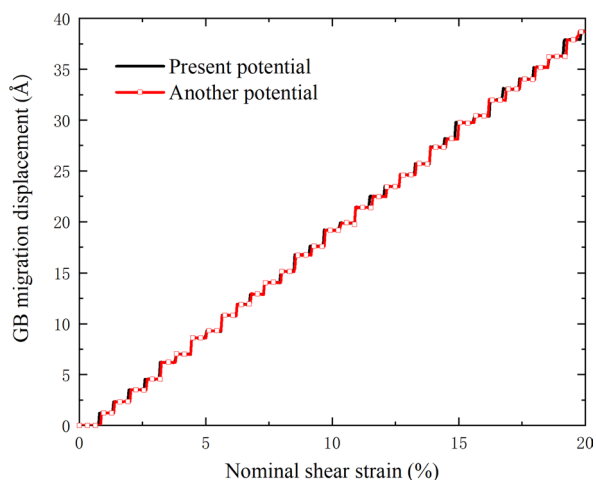


**Figure 10:** GB migration displacement versus nominal shear strain curves of pure bicrystal Ni for two different potentials.

selected and their average  $Y$  coordinate variations were captured as the GB migration displacement.

All the MD simulations were performed by using the large-scale atomic/molecular massively parallel simulator (LAMMPS) package [53] with an integration time step of 1 fs. An embedded atom method (EAM) potential [51] was used to describe the Ni–Ni, Ni–Cr, Ni–Co, Ni–Cu and Ni–Fe interactions. To check whether this potential is suitable for describing GB migration behavior well, it was compared with another commonly used potential for Ni [29, 33, 34, 54, 55] through simulating the shear-coupled GB migration of pure bicrystal Ni. As shown in Fig. 10, their GB migration displacement curves are very consistent. It reveals that the EAM potential is reliable.

Several layers of atoms in the top of the upper grain and in the bottom of the lower grain are set as two loaded slabs. A monotonically increasing shear strain with a strain rate of  $2 \times 10^8 \text{ s}^{-1}$  was applied in the  $X$  direction by moving the upper slabs. The canonical NVT ensemble with a constant number of atoms, volume and temperature [20, 33, 34, 52, 55] was employed in the simulations. It can eliminate the volume change effect during loading.

The three-dimensional visualization software OVITO [56] was used to visualize the calculation results. The common neighbor analysis method [57] was used to identify the atomic configurations. All the atoms were colored according to their configurations.

## Acknowledgments

This work was supported by the National Natural Science Foundation of China (Grant Numbers: 11772137 and 11572135) and the Fundamental Research Funds for Central Universities (No. 2662017QD018).

## Supplementary information

The online version contains supplementary material available at <https://doi.org/10.1557/s43578-020-00030-3>.

## References

1. K.S. Kumar, H. Van Swygenhoven, S. Suresh, Mechanical behavior of nanocrystalline metals and alloys The Golden Jubilee Issue—Selected topics in Materials Science and Engineering: Past, Present and Future, edited by S Suresh. *Acta Mater.* **51**, 5743 (2003)
2. M.A. Meyers, A. Mishra, D.J. Benson, Mechanical properties of nanocrystalline materials. *Prog. Mater. Sci.* **51**, 427 (2006)
3. M. Dao, L. Lu, R. Asaro, J. Dehossan, E. Ma, Toward a quantitative understanding of mechanical behavior of nanocrystalline metals. *Acta Mater.* **55**, 4041 (2007)
4. S.N. Mathaudhu, B.L. Boyce, Thermal stability: the next frontier for nanocrystalline materials. *JOM* **67**, 2785 (2015)
5. A.R. Kalidindi, T. Chookajorn, C.A. Schuh, Nanocrystalline materials at equilibrium: a thermodynamic review. *JOM* **67**, 2834 (2015)
6. H.R. Peng, M.M. Gong, Y.Z. Chen, F. Liu, Thermal stability of nanocrystalline materials: thermodynamics and kinetics. *Int. Mater. Rev.* **62**, 303 (2016)
7. D. Raabe, M. Herbig, S. Sandlöbes, Y. Li, D. Tytko, M. Kuzmina, D. Ponge, P.P. Choi, Grain boundary segregation engineering in metallic alloys: a pathway to the design of interfaces. *Curr. Opin. Solid State Mater. Sci.* **18**, 253 (2014)
8. F. Abdeljawad, S.M. Foiles, Stabilization of nanocrystalline alloys via grain boundary segregation: a diffuse interface model. *Acta Mater.* **101**, 159 (2015)
9. T. Chookajorn, H.A. Murdoch, C.A. Schuh, Design of stable nanocrystalline alloys. *Science* **337**, 951 (2012)
10. A. Detor, C. Schuh, Tailoring and patterning the grain size of nanocrystalline alloys. *Acta Mater.* **55**, 371 (2007)
11. A.J. Detor, C.A. Schuh, Microstructural evolution during the heat treatment of nanocrystalline alloys. *J. Mater. Res.* **22**, 3233 (2007)
12. A.J. Detor, M.K. Miller, C.A. Schuh, Solute distribution in nanocrystalline Ni–W alloys examined through atom probe tomography. *Philos. Mag.* **86**, 4459 (2006)
13. L. Zheng, G. Schmitz, Y. Meng, R. Chellali, R. Schlesiger, Mechanism of intermediate temperature embrittlement of Ni and Ni-based superalloys. *Crit. Rev. Solid State Mater. Sci.* **37**, 181 (2012)
14. J.D. Schuler, O.K. Donaldson, T.J. Rupert, Amorphous complexions enable a new region of high temperature stability in nanocrystalline Ni–W. *Scripta Mater.* **154**, 49 (2018)

15. V. Borovikov, M.I. Mendeleev, A.H. King, Solute effects on interfacial dislocation emission in nanomaterials: nucleation site competition and neutralization. *Scripta Mater.* **154**, 12 (2018)
16. Q. Li, J. Zhang, H. Tang, H. Ye, Y. Zheng, Regulating the mechanical properties of nanocrystalline nickel via molybdenum segregation: an atomistic study. *Nanotechnology* **30**, 275702 (2019)
17. C.J. Wang, B.N. Yao, Z.R. Liu, X.F. Kong, D. Legut, R.F. Zhang, Y. Deng, Effects of solutes on dislocation nucleation and interface sliding of bimetal semi-coherent interface. *Int. J. Plast.* **131**, 102725 (2020)
18. S. Pal, K. Vijay Reddy, D.E. Spearot, Zr segregation in Ni–Zr alloy: implication on deformation mechanism during shear loading and bending creep. *J. Mater. Sci.* **55**, 6172 (2020)
19. J. Schäfer, Y. Ashkenazy, K. Albe, R.S. Averback, Effect of solute segregation on thermal creep in dilute nanocrystalline Cu alloys. *Mater. Sci. Eng. A* **546**, 307 (2012)
20. T. Frolov, S.V. Divinski, M. Asta, Y. Mishin, Effect of interface phase transformations on diffusion and segregation in high-angle grain boundaries. *Phys. Rev. Lett.* **110**, 255502 (2013)
21. S. Yang, N. Zhou, H. Zheng, S.P. Ong, J. Luo, First-order interfacial transformations with a critical point: breaking the symmetry at a symmetric tilt grain boundary. *Phys. Rev. Lett.* **120**, 085702 (2018)
22. Y. Hu, T.J. Rupert, Atomistic modeling of interfacial segregation and structural transitions in ternary alloys. *J. Mater. Sci.* **54**, 3975 (2018)
23. K.V. Reddy, S. Pal, Effect of grain boundary complexions on the deformation behavior of Ni bicrystal during bending creep. *J. Mol. Model.* **24**, 87 (2018)
24. R. Tran, Z. Xu, N. Zhou, B. Radhakrishnan, J. Luo, O.S. Ping, Computational study of metallic dopant segregation and embrittlement at molybdenum grain boundaries. *Acta Mater.* **117**, 91 (2016)
25. J.W. Cahn, Y. Mishin, A. Suzuki, Coupling grain boundary motion to shear deformation. *Acta Mater.* **54**, 4953 (2006)
26. J.W. Cahn, J.E. Taylor, A unified approach to motion of grain boundaries, relative tangential translation along grain boundaries, and grain rotation. *Acta Mater.* **52**, 4887 (2004)
27. J.W. Cahn, Y. Mishin, A. Suzuki, Duality of dislocation content of grain boundaries. *Philos. Mag.* **86**, 3965 (2006)
28. L. Wan, S. Wang, Shear response of the  $\Sigma 11, \langle 110 \rangle \{131\}$  symmetric tilt grain boundary studied by molecular dynamics. *Model. Simul. Mater. Sci. Eng.* **17**, 045008 (2009)
29. L. Wan, S. Wang, Shear response of the  $\Sigma 9 \langle 110 \rangle \{221\}$  symmetric tilt grain boundary in fcc metals studied by atomistic simulation methods. *Phys. Rev. B* **82**, 045008 (2010)
30. L. Wan, W. Han, K. Chen, Bi-crystallographic lattice structure directs grain boundary motion under shear stress. *Sci. Rep.* (2015). <https://doi.org/10.1038/srep13441>
31. L. Zhang, C. Lu, G. Michal, K. Tieu, K. Cheng, Molecular dynamics study on the atomic mechanisms of coupling motion of  $[001]$  symmetric tilt grain boundaries in copper bicrystal. *Mater. Res. Exp.* **1**, 015019 (2014)
32. L. Zhang, C. Lu, K. Tieu, X. Zhao, L. Pei, The shear response of copper bicrystals with  $\Sigma 11$  symmetric and asymmetric tilt grain boundaries by molecular dynamics simulation. *Nanoscale* **7**, 7224 (2015)
33. P. Wang, X. Yang, D. Peng, Initiation, evolution, and saturation of coupled grain boundary motion in nanocrystalline materials. *Comput. Mater. Sci.* **112**, 289 (2016)
34. X. Yang, J. Li, P. Wang, Grain boundary migration in nanocrystalline Ni under constant shear strains and its mechanism. *Comput. Mater. Sci.* **176**, 109530 (2020)
35. K. Lücke, K. Detert, A quantitative theory of grain-boundary motion and recrystallization in metals in the presence of impurities. *Acta Metall.* **5**, 628 (1957)
36. J.W. Cahn, The impurity-drag effect in grain boundary motion. *Acta Metall.* **10**, 789 (1962)
37. M. Hillert, B. Sundman, A treatment of the solute drag on moving grain boundaries and phase interfaces in binary alloys. *Acta Metall.* **24**, 731 (1976)
38. J. Schäfer, K. Albe, Competing deformation mechanisms in nanocrystalline metals and alloys: coupled motion versus grain boundary sliding. *Acta Mater.* **60**, 6076 (2012)
39. J. Schäfer, K. Albe, Influence of solutes on the competition between mesoscopic grain boundary sliding and coupled grain boundary motion. *Scripta Mater.* **66**, 315 (2012)
40. K.A. Darling, R.N. Chan, P.Z. Wong, J.E. Semones, R.O. Scattergood, C.C. Koch, Grain-size stabilization in nanocrystalline FeZr alloys. *Scripta Mater.* **59**, 530 (2008)
41. A. Detor, C. Schuh, Grain boundary segregation, chemical ordering and stability of nanocrystalline alloys: atomistic computer simulations in the Ni–W system. *Acta Mater.* **55**, 4221 (2007)
42. P.C. Millett, R.P. Selvam, A. Saxena, Molecular dynamics simulations of grain size stabilization in nanocrystalline materials by addition of dopants. *Acta Mater.* **54**, 297 (2006)
43. J. Han, S.L. Thomas, D.J. Srolovitz, Grain-boundary kinetics: a unified approach. *Prog. Mater. Sci.* **98**, 386 (2018)
44. Q. Zhu, G. Cao, J. Wang, C. Deng, J. Li, Z. Zhang, S.X. Mao, In situ atomistic observation of disconnection-mediated grain boundary migration. *Nat. Commun.* **10**, 156 (2019)
45. A. Rajabzadeh, F. Mompou, S. Lartigue-Korinek, N. Combe, M. Legros, D.A. Molodov, The role of disconnections in deformation-coupled grain boundary migration. *Acta Mater.* **77**, 223 (2014)
46. S. Sanyal, U.V. Waghmare, P.R. Subramanian, M.F.X. Gigliotti, Effect of dopants on grain boundary decohesion of Ni: a first-principles study. *Appl. Phys. Lett.* **93**, 223113 (2008)



47. X. Zhou, J. Song, Effects of alloying elements on vacancies and vacancy-hydrogen clusters at coherent twin boundaries in nickel alloys. *Acta Mater.* **148**, 9 (2018)
48. L. Zhu, J. Zhou, H. Yang, Z. Sun, Energetics and kinetics of hydrogen at the grain boundary of the Ni alloys: a first-principles study. *J. Alloys Compd.* **795**, 343 (2019)
49. F.A.M. Ahmed, H.-T. Xue, F.-L. Tang, J.-P. An, Y.-Q. Luo, X.-F. Lu, J.-Q. Ren, Segregation of alloying elements and their effects on the thermodynamic stability and fracture strength of  $\gamma$ -Ni/ $\gamma'$ -Ni<sub>3</sub>Al interface. *J. Mater. Sci.* **55**, 12513 (2020)
50. G. Arora, K.D. Rawat, D.S. Aidhy, Effect of atomic order/disorder on Cr segregation in Ni-Fe alloys. *J. Appl. Phys.* **124**, 115303 (2018)
51. D. Farkas, A. Caro, Model interatomic potentials and lattice strain in a high-entropy alloy. *J. Mater. Res.* **33**, 3218 (2018)
52. P.C. Millett, R.P. Selvam, A. Saxena, Improving grain boundary sliding resistance with segregated dopants. *Mater. Sci. Eng. A.* **431**, 92 (2006)
53. P. Steve, Fast parallel algorithms for short-range molecular dynamics. *J. Comput. Phys.* **117**, 1 (1995)
54. Y. Mishin, D. Farkas, M.J. Mehl, D.A. Papaconstantopoulos, Interatomic potentials for monoatomic metals from experimental data and ab initio calculations. *Phys. Rev. B* **59**, 3393 (1999)
55. P. Wang, X. Yang, D. Peng, Molecular dynamics investigation of the grain boundary migration hysteresis of nanocrystalline Ni under cyclic shear loading. *Model. Simul. Mater. Sci. Eng.* **25**, 025006 (2017)
56. A. Stukowski, Visualization and analysis of atomistic simulation data with OVITO—the open visualization tool. *Model. Simul. Mater. Sci. Eng.* **18**, 015012 (2010)
57. D. Faken, H. Jonsson, Systematic analysis of local atomic structure combined with 3D computer graphics. *Comput. Mater. Sci.* **2**, 279 (1994)